


Green Synthesis of Silver Nano-particles by *Macrococcus bovicus* and Its Immobilization onto Montmorillonite Clay for Antimicrobial Functionality

Mohamed S. Abdel-Aziz¹ · Khaled S. Abou-El-Sherbini²  · Esmat M. A. Hamzawy³ · Mohey H. A. Amr⁴ · Shady El-Dafrawy⁵

Received: 23 March 2015 / Accepted: 8 June 2015 /
Published online: 23 June 2015
© Springer Science+Business Media New York 2015

Abstract *Macrococcus bovicus* was locally isolated from soil and used in the green synthesis of nano-scaling silver (NSAg). It was immobilized on a sodic-montmorillonite clay (MMT1) and cetyltrimethylammonium bromide-modified montmorillonite (MMT2) which was also calcined at 300 °C (MMT3). The NSAg clays were characterized by X-ray fluorescence, Fourier transform infrared spectra, X-ray diffractometry, surface area measurement, UV–Vis spectrometry, scanning electron microscope, transmission electron microscope and thermogravimetric analysis. NSAg was confirmed to be included in the interparticular cavities of the clay sheets and its mechanical stability was evidenced. The antimicrobial activity of the NSAg-modified clays was investigated against *Staphylococcus aureus*, *Escherichia coli* and *Candida albicans* using the cup plate and the plate count techniques. The antimicrobial activity of the NSAg clays was confirmed and attributed to the caging of NSAg in MMT cavities. MMT3 was found to inhibit the microbial growth to as high as 65 % as observed from the plate count method.

Keywords Biosynthesis · Nano-silver · Immobilization · Montmorillonite · Antimicrobial activity

✉ Khaled S. Abou-El-Sherbini
kh_sherbini@yahoo.com

¹ Department of Microbial Chemistry, National Research Centre, 33 El Bohouth St., (former Tahrir St.), Dokki, Cairo 12622, Egypt

² Department of Inorganic Chemistry, National Research Centre, 33 El Bohouth St., (former Tahrir St.), Dokki, Cairo 12622, Egypt

³ Department of Glass, National Research Centre, 33 El Bohouth St., (former Tahrir St.), Dokki, Cairo 12622, Egypt

⁴ Research Department, Trace Elements Laboratory, Chemistry Administration, 12 Ramsis St., Cairo, Egypt

⁵ Department of Chemistry, Faculty of Science, Mansoura University, Mansoura, Egypt

Introduction

Many people worldwide lack safe drinking water, and at least five million deaths per year can be attributed to water-borne diseases [1]. Water pollution, therefore, is a serious global issue particularly in Africa and the Middle East countries because of drought. Infectious diseases caused by pathogenic bacteria, viruses and parasites are the most common and widespread health risk associated with drinking water [2]. Consequently, it is of great priority, particularly in water-poor countries to enable simple disinfection techniques of fresh water supplies for various purposes.

Classical disinfection methods have serious disadvantages. For example, chlorination, the most used drinking water disinfectant for its low cost and fast kinetics, produces residual free and combined chlorine [3]. Another disadvantage of chlorination is that some pathogens are Cl_2 resistant and/or convert to antibiotic resistant after treatment such as *Staphylococcus aureus* [4].

Recently, nano-materials particularly nano-scaling silver (NSAg) [5–11] showed a broad spectrum antimicrobial functionality towards microorganisms. The particle size of the nano-metal plays an important role in the antimicrobial activity. That were observed in the influence of particle size and shape of NSAg nano-particle on HIV-1 virus replication (10 nm) [5], pathogenic fungi (13.5 nm) [6], common fungi (58 nm) [7] and biofilms (9.3–35 nm) [9–11].

There are an extensive number of chemical, physical and biological synthesis methods of NSAg that are readily available in the literature [10, 12]. Currently, there is a growing need to adopt eco-friendly processes for nano-particle synthesis, and hence the focus turned towards 'green' chemistry and bioprocesses [13–16]. Biological methods in particular are currently gaining importance because they are cost effective and do not involve the use of any toxic chemicals for the synthesis of nano-materials. They are safer alternatives to physical and chemical methods, which involves harsh conditions and use of hazardous chemicals [8, 10, 12]. For instance, spent mushroom substrate has been used to reduce ionic silver to NSAg and further provides stabilization to nano-silver suspensions [13]. Furthermore, NSAg is successfully produced by microorganisms including bacteria [14] and fungi [15, 16]. For example, extracellular NSAg (diameter 5–25 nm) was synthesized using *Aspergillus fumigatus* [15] and non-pathogenic fungus *Trichoderma asperellum* [16]. One possible (passive) role of the microorganisms is in providing a multitude of nucleation centres, establishing conditions for obtaining highly dispersed nano-particle systems. In addition, they slow down aggregation, or entirely prevent it by immobilizing the particles, providing naturally-occurring end-capping materials and viscous medium [17].

The wide application of nano-materials (NMs) is obstructed by many obstacles such as the difficulty of manipulating the suspension, the ultimate health risks of the dissipation of nano-particles to environment [18], instability of size due to aggregation, and the effect of the suspension-stabilizing agent [10, 12]. Coating quantum dot nano-crystals with polyethylene glycol suppressed agglomeration and stabilized the suspension regardless of the ionic strength [19]. Branched polyethyleneimine (BPEI) stabilized NSAg [20].

Although the stability of the produced colloidal NSAg dispersions have been partially solved by the use of organic supporting materials such as textile or cellulose, practice shows the loss of the NSAg with usage [21]. Some brands of socks were shown to lose nearly all of their NSAg content, added to kill bacteria, within a few washings [21]. Moreover, to get use of NMs, it is not possible to cage them in rigid confinements restricting their access to microorganisms which ranges from 1 to 10 nm for the viruses to micrometre range in case of bacteria.

Recently, Ag^+ was intercalated into montmorillonite (MMT) [22, 23] and MMT modified with sulphur amino acids [24] then reduced to form NSAg and used as antimicrobial agents.

MMT was used as NM support for its hosting capability of its inert rigid two-dimensional network of aluminosilicate layers.

NSAg was not directly immobilized on MMT yet. The present study demonstrates (1) the isolation of the bacteria *Macrocooccus bovicus* from local soil, (2) the synthesis of NSAg using *M. Bovicus* and (3) the direct immobilization of NSAg on MMT, as an inorganic support, and the study of its antimicrobial activity.

Experimental

Materials

Bacterial Isolation

Soil sample collected from agricultural environment (Mansoura, Lower Egypt), using sterile plastic bag, was shifted to the laboratory within 3 h. One gram of soil was added to 9 mL of sterile saline solution (0.85 w/v) and shaken for 2 h and then left to stand for 15 min. A serial dilution up to 10^{-7} had been done. From the last four dilutions (10^{-4} to 10^{-7}), 200 μ L were used to inoculate Petri dishes (15-cm diameter), each containing 50 mL of nutrient agar medium. Dishes were incubated at 30 °C for 24 and 48 h (or more). The appeared bacterial colonies were picked up and maintained on nutrient agar slants till next use. The bacterial isolate that used in this work was identified using carbon substrate utilization and biochemical test. The bacterial isolate was characterized by means of sole carbon source utilization profiles using the Biolog GN Microplates (Biolog GN2, UK) according to the manufacturers' instructions. Twenty-four-hour-old isolates grown on King's B medium were homogeneously suspended in sterile distilled water (DW) before inoculation on the profiles. Results of the Biolog GN Microplates were recorded after 24- and 48-h incubation at 26 °C. Biochemical reactions were visually observed and subjected to a micro-titre plate reader (Bio-Tek ELx 800) at 620-nm absorbance level. Data were entered into Bionumerics software (version 4.5) and subjected to cluster analysis using the unweight pair group-average method (UPGMA). The identity of isolates were further confirmed using the Analytical Profile Index, API 20E (bioMerieux, Marcy l'Etoile, France), according to the manufacturers' instructions. Homogeneous suspensions (1×10^6) were inoculated in the tube of API 20E kits. Data were recorded after 24-h incubation at 26 °C and seven-digit profiles developed for every isolate. Profiles were identified using the APILAB version 4.1 identification program (BioMérieux).

MMT Montmorillonite Clay

MMT (procured from Sinai, Egypt) contains SiO₂, 52.56 %; Al₂O₃, 18.49 %; Fe₂O₃, 13.44 %; MgO, 2.44 %; CaO, 1.11 %; Na₂O, 1.24 %; K₂O, 1.38 %; TiO₂, 2.06 %; Cl, 0.708 %; P₂O₅, 0.159 %; SO₃, 0.161 %; and LOI, 6.1 % as determined by X-ray fluorescence (XRF). The basal spacing (d_{001}) of the air-dried MMT was about 15.16 Å that suggests it is a calcic MMT.

Other reagents were of analytical-grade purity, unless otherwise stated.

Instrumentation

The bacterial isolate was identified by using the Biolog (GN2, UK) instrument. XRF analysis was performed on X-ray fluorescence analysis (ARL 72000, Switzerland). IR spectra were recorded

on KBr discs in a Perkin-Elmer system 2000 FTIR spectrophotometer. Powder X-ray diffraction (XRD) was recorded on a Bruker AXS D8 ADVANCE using $\text{Cu}_{\text{K}\alpha}$ source ($\lambda = 1.5406 \text{ \AA}$). Specific surface area, pore volume and average pore diameter were measured with Quantachrome USA NOVA 22. The UV–visible absorption spectra for the aqueous dispersions were recorded at room temperature on a Shimadzu UV–VIS 2401PC spectrophotometer using a 1-cm quartz cuvette. The scanning electron microscope (SEM) images were performed using SEM model Quanta 250 field emission gun (FEG) attached with EDX Unit (energy-dispersive X-ray analyses), with accelerating voltage 30 kV, magnification $\times 14$ up to 1,000,000 and resolution for Gun. In, FEI Company, Netherlands. The transmission electron microscopy (TEM) analysis of extracellular synthesized NSAg were prepared by drop-coating biosynthesized NSAg solution on carbon-coated copper TEM grids ($40 \mu\text{m} \times 40 \mu\text{m}$ mesh size). Samples were dried and kept under vacuum in desiccators before loading them onto a specimen holder. TEM measurements were performed on a JEOL model 1200EX electron microscope operated at an accelerating voltage at 120 kV. Elemental analysis of Ag was performed using atomic absorption spectrometry (AAS) on Perkin Elmer Analyst 800, USA. The samples used in AAS were digested in HF/HNO_3 in Milestone MLS Ethos 900 Plus Microwave.

Methodology

Growth Conditions

Macrococcus bovicus stock cultures were maintained by subculturing at monthly intervals on nutrient agar medium. One-litre Erlenmeyer conical flasks containing 200 mL of nutrient broth medium was inoculated with a loopful of bacterial cells and incubated for 48 h at 37°C with shaking at 160 rpm. After incubation period, the cultures were centrifuged at 8000 rpm for 10 min and the supernatant were collected.

Biosynthesis of Nano-silver

For the biosynthesis of NSAg, 50-mL aqueous solution of 3 mM silver nitrate (AgNO_3) was added to 50 mL of *M. bovicus* supernatant solution in a 250-mL Erlenmeyer flask. The whole mixture was put into a shaker at 40°C (200 rpm) for 5 days and maintained in the dark. Control experiments were conducted with uninoculated media, to check for the role of bacteria in the synthesis of nano-particles. The reduction of Ag^+ ions was recorded by noticing colour change from yellow to reddish brown colour and sampling an aliquot (2 mL) of the solution at intervals of 24 h and measuring the UV–Vis spectra of the solution.

Preparation of Montmorillonite Clay MMT

MMT was converted into the homoionic Na-exchanged form by stirring 50 g in 1 L of 1 mol L^{-1} NaCl solution for about 24 h, washed by centrifuge until the conductivity of the water approached that of DW. The clay suspension (50 g in 500 mL H_2O) was oxidized with 50 mL 30 % H_2O_2 at 50°C for 48 h till near dryness to digest organic matter. The slurry was diluted to 1400 mL and purified by sedimentation according to Gillott [25], to collect the $<2 \mu\text{m}$ fraction before use and to discard 3D crystalline components. Final composition of the clay suspension was 2.66 g/100 mL and used as it is for immobilization experiments. For analysis, 100 mL of the clay suspension was dried at 50°C for 48 h and named MMT-pure.

Cation exchange capacity (CEC) was estimated by the ammonium acetate method. MMT-pure was first saturated by ammonium acetate to exchange the interlayer cation by the ammonium ion method [26]. Excess ammonium was determined in the liquor by Kjeldahl method. The CEC was determined to be 91.7 mEq per 100 g of the clay. The specific surface area of MMT-pure, determined by N₂ adsorption, was 24.5 m² g⁻¹.

Immobilization of NSAg on MMT

A volume of 100 mL of the NSAg suspension was added to 200 mL of the clay suspension and stirred for 24 h at room temperature. Then the suspension was centrifuged at 8000 rpm for 10 min, washed with DW, dried at 50 °C for 48 h and labelled MMT-Ag1.

A 1.82-g cetyltrimethylammonium bromide (CTAB) was added to 200 mL of the clay suspension and stirred for 24 h at room temperature. This is equivalent to the CEC of the montmorillonite. Then 100 mL of the NSAg suspension was added to the suspension, stirred for 24 h centrifuged at 8000 rpm for 10 min, washed with DW, dried at 50 °C for 48 h and named MMT-Ag2. Then, MMT-Ag2 was calcined at 300 °C for 3 h in air and named MMT-Ag3.

A 1.82-g CTAB was added to 200 mL of the clay suspension and stirred for 24 h at room temperature. Then, the suspension was stirred for 24 h, centrifuged at 8000 rpm for 10 min, washed with DW, dried at 50 °C for 48 h and named MMT-CTAB.

Antimicrobial Activity of NSAg-Modified MMT Clay

The antimicrobial activity of the modified clays was firstly studied using cup plate method. The selected test strains of bacteria (G+ve, *S. aureus*, and G-ve, *Escherichia coli*) and yeast (*Candida albicans*) were inoculated into 20 mL of sterile nutrient broth and incubated at 37 °C for 16–18 h. Using a sterile cotton swab, the nutrient broth cultures were swabbed on the surface of sterile nutrient agar plates. Agar wells were prepared with the help of sterilized cork borer with 10-mm diameter [27]. Using a micropipette, 100-μl suspensions of treated and control MMT clay were added to different wells in the plate. The plates were incubated in an upright position at 37 °C for 24 h. The diameter of inhibition zones was measured in millimetre and the results were recorded.

Then the antimicrobial activity of MMT3 was studied using plate count technique by measuring the colony forming unit (CFU) method. The bacteria from the stock culture, *S. aureus*, were inoculated into a freshly prepared liquid nutrient broth containing 5 g L⁻¹ peptone and 3 g L⁻¹ beef extract at pH 6.8 and incubated for 24 h. Samples were added to the inoculated flasks leaving the control (untreated sample). After 16-h incubation at 37 °C, a serial dilution from each sample-containing culture and the control has been done (10⁻²–10⁻⁷). The microbial inhibition was determined by two methods. Firstly, the CFU by inoculating Petri dishes containing solidified nutrient agar medium with 100 μl from each dilution are counted and the reduction growth rate (*R*) for treated samples in relation to control (untreated) are calculated according to Eq. 1:

$$R (\%) = \frac{B - A}{B} \times 100 \quad (1)$$

where *A* is CFU/mL for treated sample after 16-h incubation and *B* is CFU/mL for untreated sample after the same period of incubation time [28].

In the second method, the optical density of the incubation liquid culture medium was recorded at 660 nm. The greater the growth, the higher the turbidity, and the optical density figure was directly proportional to the number of the bacteria in the medium.

Results and Discussion

Characterization of NSAg

The bacterial isolate was identified as *M. bovicus*. Members of the *Macrococcus* genus belongs to Gram-positive cocci, family *Staphylococcaceae*, non-motile, non-spore forming that are coagulase negative and catalase positive. They can be distinguished phenotypically from most staphylococci on the basis of their cellular morphology being are 2.5–4 times larger in diameter compared to *S. aureus*. When *M. bovicus* culture supernatant was mixed with an equal amount of aqueous solution of silver nitrate (3 mmol L^{-1}), a reddish brown colour was formed as an indication of NSAg formation. Figure 1 shows the colour change of *M. bovicus* bacterial culture and silver nitrate-treated culture filtrates from yellow to reddish brown attributed to the formation of NSAg. The UV–visible spectra (Fig. 2) show two broad absorption bands entered at about 389 and 455 nm. These bands are associated with the absorption by surface plasmons in NSAg (red coloured) [29]. According to Mie [30], if the particles do not interact, the width of the absorption band is inversely proportional to the size of the particles indicating that it is in the nano-range. TEM investigation of the NSAg suspension of dead culture (Fig. 3) shows the accumulation of NSAg with a size range ~5.4–21.5 nm in the form of aggregates. The morphology of the nano-particles is highly

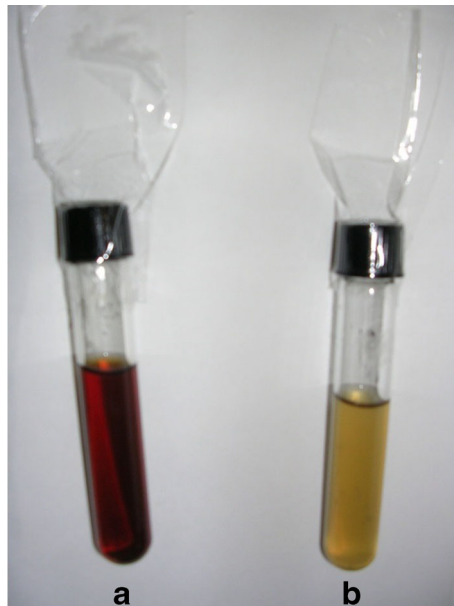


Fig. 1 The colour change of *Macrococcus bovicus* bacterial culture and silver nitrate-treated culture filtrate (NSAg). Silver nano-particles (reddish brown) (a), culture filtrate (yellow) (b)

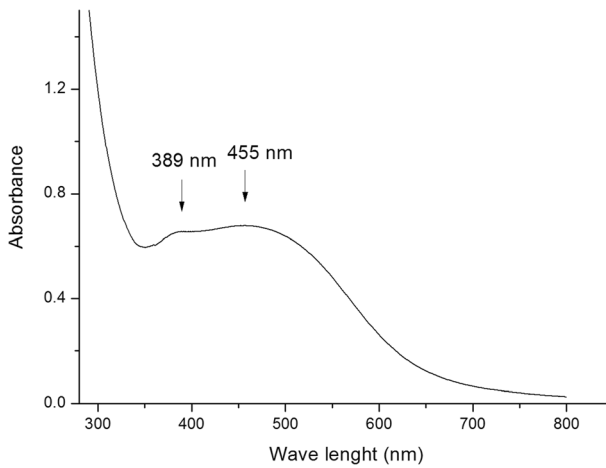


Fig. 2 UV–Vis spectrometry of aqueous NSAg synthesized by *M. bovicus* culture supernatant

variable. The nano-particles were not in direct contact even within the aggregates, indicating stabilization of the nano-particles by a capping agent. The separation between the NSAg seen in the TEM image (Fig. 3) could be due to the capping by proteins. This is in agreement with

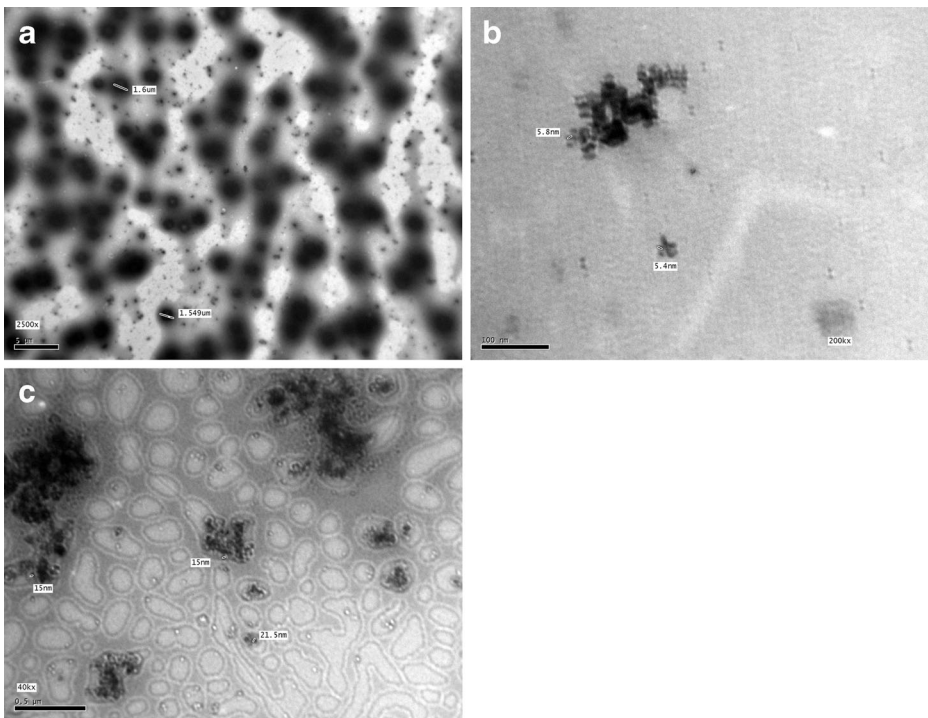


Fig. 3 TEM micrographs recorded from a drop-coated film of an aqueous solution of *Macrocooccus bovicus* culture supernatant reacted with 3 mM Ag^+ ions for 96 h at 30 °C (a–c)

previous results [31] which reported that Ag^+ is reduced during the metabolism of anaerobic cultures of *Shewanella oneidensis* in presence of high Ag^+ concentrations (100 μM) and the NSAg forms in aggregates.

The crystalline nature of the Ag nano-particles was also confirmed by the powder XRD pattern (Fig. 4). The reflection at $2\theta = 38.069^\circ$ was assigned to the (111) of a cubic face-centred (fcc) lattice of silver (PDF 87-0720 silver 3C) whereas the (200) and (220) diffractions were hardly seen, probably due to the small size of the NSAg. This result also substantiated the TEM and UV results.

Immobilization of NSAg on MMT

As the surface of the MMT is hydrophilic, due to the presence of Na cations in the interlayer space and the surface OH terminals, the NSAg particles may not better be dispersed in the MMT particles. The exchange of the Na cations by an organic cation, such as cetyltrimethylammonium cation (CTA^+), is of great importance to render the clay surface partially organophilic which eases the dispersion of NSAg (covered with cell contents [13]) in the pores of CTA-modified MMT. This modification is also intended to ease mutual access of microorganisms and NSAg immobilized on organo-modified clay due to high homogeneity and remarkable improvements in diffusion properties [32].

Elemental analysis of Ag indicated that its concentration in MMT1, MMT2 and MMT3 was 0.042, 0.106 and 0.126 % giving an efficiency of immobilization of 13.8, 44.2 and 41.4 % of the actually added NSAg/clay percentage; 0.304, 0.24 and 0.304 %. The apparent increase in Ag content in MMT2 and MMT3 in comparison with MMT1 may be attributed to the organo-functionalization of MMT2 that helped in capturing the NSAg in the clay phase.

The powder XRD patterns of MMT and its modified phases are shown in Fig. 5. MMT shows the presence of a main phase of Ca-montmorillonite, PDF 13-259; a lesser abundant phase quartz, PDF 5-490; and minor phases of kaolinite, PDF 14-164, and albite, PDF 1-739. The basal interlayered spacing (d_{001}) of MMT is found to be 15.16 Å which indicates a hydrated calcic MMT [33]. Preliminary sedimentation, Na exchange and oxidation lead to the exclusion of the kaolinite and albite phases and the minimization of the quartz phase with a

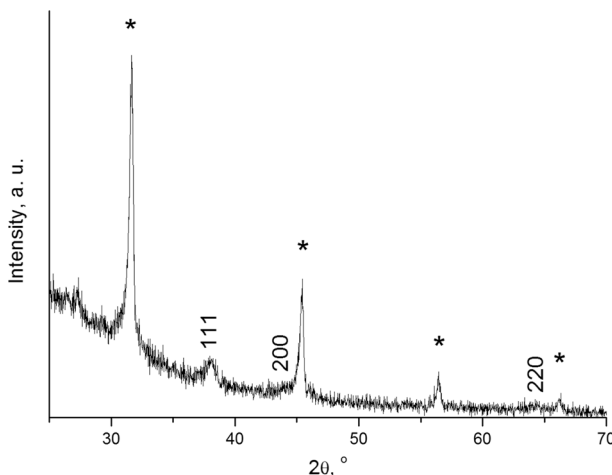


Fig. 4 Powder XRD pattern of NSAg. Asterisk denotes NaCl (Halite 88-2300) residual from culture salts

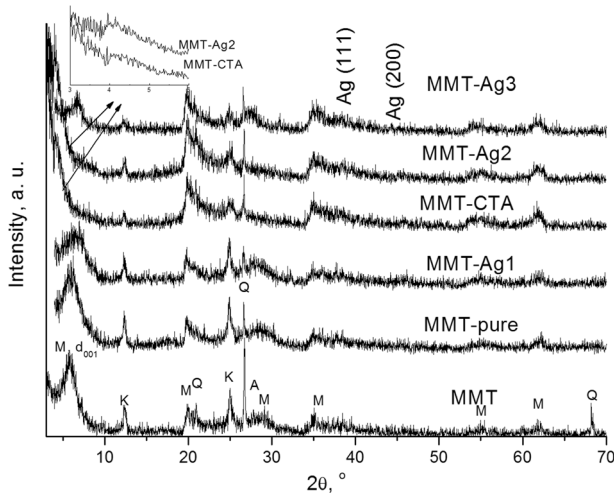


Fig. 5 Powder XRD pattern of NSAg. *M* montmorillonite (13–259), *K* kaolinite (14–164), *A* albite (1–739), *Q* quartz, low (5–490)

change in the basal interlayered spacing of MMT-pure (14.23 \AA , $2\theta 6.208^\circ$) which is in accordance with that reported for Na-MMT [33].

The direct addition of NSAg to MMT-pure does not affect its structure and no lines from Ag can be detected in the diffractogram of MMT-Ag1 which may be likely due to the presence of the finally divided NSAg in small concentration.

CTA⁺-intercalated MMT samples, MMT-CTAB and MMT-Ag2, show a large increase in the interlayered spacing to 21.33 and 21.84 \AA ($2\theta 4.14^\circ$ and 4.04°), respectively, indicating the intercalation of CTA⁺ cation replaced with Na⁺. This basal spacing is in accordance with a tilted mono paraffinic arrangement [34]. The angle between the CTA⁺ cation and the MMT base could be calculated to be 37.5° and 38.6° taking into account the length of CTA⁺ cation and the aluminosilicate MMT layer (25 and 9.7 \AA , respectively) [35]. The d_{001} reflection of MMT-CTA⁺ and MMT2 is broad and weak which may be due to the waving of aluminosilicate layers. No indication of the insertion of NSAg in the Van der Waal's gap of MMT3 could be observed as confirmed by the recovery of a close interlayered spacing of MMT (13.56 \AA , $2\theta 6.515^\circ$) after the combustion of most of the organic substrate. Actually, complete combustion should have produced d_{001} at 9.7 \AA which is the thickness of the aluminosilicate layer in MMT [34]. This was deliberately avoided as the nano-composite would lose its mobility [36] which is needed for the mutual accessibility of NSAg and microorganisms on application as antimicrobe. Weak XRD reflections are observed at $2\theta 38.39$ and 44.35° in MMT-Ag3 diffractogram which may be due to the (111) and (200) lines of Ag, respectively.

FTIR studies on clay composites (Table 1) indicated that NSAg does not affect the MMT structure. The intercalation of MMT with CTA⁺ cation is confirmed by the observation of δ_{C-H} and symmetric and asymmetric ν_{CH_2} in the FTIR spectra of MMT-CTA⁺ and MMT2 [40]. The intercalation is observed to be accompanied by a decrease in the water content as concluded from the decrease in the intensity of ν_{OH} . The weak band at 2923 cm^{-1} , attributed to the asymmetric ν_{CH_2} , and the development of a band attributed to ν_{CO} for MMT3 are due to residual organic constituent. This means that thermal treatment of MMT2 leads to an incomplete combustion of the organic content. The blue shift of the band assigned to asymmetric

Table 1 Infrared spectra (cm^{-1}) of clay composites

Type of vibration	Wave number					Reference
	MMT-pure	MMT1	MMT-CTAB	MMT2	MMT3	
Tetrahedral $\delta_{\text{Si-O-Si}}$	428	420	424	423	412	[37]
Tetrahedral $\delta_{\text{Si-O-Mg}}$	469	468	468	466	468	[37]
Tetrahedral $\delta_{\text{Si-O-Al}}$	526	527	527	524	529	[37]
Kaolin	69-	693	695	695	–	[38]
Deformation vibration of hydroxyls in [Fe(III) Fe(III)-OH] and [Fe(III)Mg-OH]	795	795	796	795	794	[38]
–	–	834	835	–	–	–
Smectite 2:1 deformation Al–Al–OH	912	912	912	912	912	[37]
ν_{SiO}	1035	1032	1032	1032	1032	[37]
Symmetric $\delta_{\text{C-H}}$ of alkylammonium groups	–	–	1471	1471	–	[39, 40]
δ_{OH}	1643	1641 (s)	1639 (m)	1639 (m)	1635 (s)	[39]
ν_{CO}	–	–	–	–	1700	[39]
Symmetric ν_{CH_2}	285-	2853 (vw)	2851 (s)	2851 (s)	–	[39]
Asymmetric ν_{CH_2}	292-	2925 (vw)	2920 (s)	2920 (s)	2923 (w)	[39]
ν_{OH}	3434	3422 (vs)	3425 (s)	3432 (s)	3444 (m)	[37]
$\nu_{\text{Al-OH}}$	3621	3622	3622	3621	3621	[38]
$\nu_{\text{Al-OH}}$ in kaolinite	3697	3697	3697	3696	3697	[38]

vs very strong, *s* strong, *m* medium, *w* weak, *vw* very weak

ν_{CH_2} in MMT-CTAB and MMT2 compared to MMT1 and MMT3 indicates that the intercalated CTA^+ cations are ordered [41]. The hydrophilic character of modified clays, which is necessary when dealing with aqueous environments, is still evident as seen from the presence of the bands due to adsorbed water ν_{OH} and δ_{OH} .

TGA of MMT and MMT2 is shown in Fig. 6. The TGA curves show the total weight loss of MMT and MMT2 as 17.0 and 32.3 %, respectively, in the range from room temperature to 700 °C. MMT shows two weight loss stages with onsets at 70.0 (11.4 %) and 547.0 °C (5.49 %) attributed to the loss of water (adsorbed and intercalated) and dehydroxylation of surface silanol and aluminol groups, respectively, whereas MMT2 shows four stages with onsets at 43.0 (2.41 %), 213.0 (17.9 %), 466 (6.0 %) and 556 (6.2 %). The first stage is attributed to the loss of adsorbed water whereas the next two may be due to the loss of adsorbed CTAB and electrostatically bonded CTA^+ (49.1 and 21.1 mEq of each, respectively). This may indicate that only 23 % of the CEC of MMT is utilized which may be attributed to the steric hindrance from organic substrates. The last stage is attributed to the dehydroxylation of surface silanol and aluminol bonds [42]. The large decrease of the water loss stage in MMT2 compared with MMT associated with a shift to lower temperature onset indicates the loss of intercalated water that displaced by the hydrophobic CTA^+ and CTAB.

Surface area measurements of MMT and its modified phases (Table 2) showed a tenfold increase in S_{BET} for MMT after organo-functionalization with CTAB indicating the

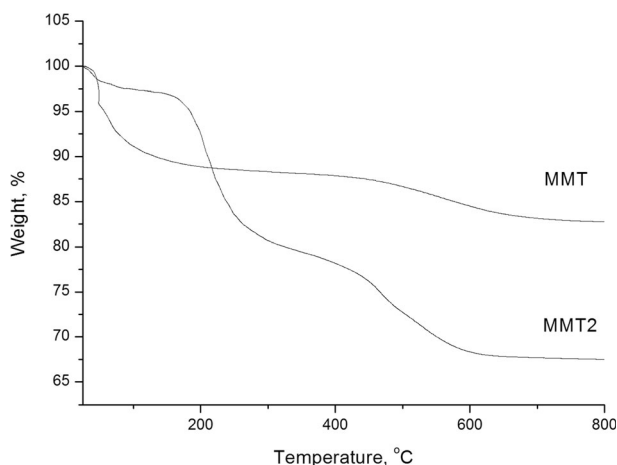


Fig. 6 Thermogravimetric analysis of MMT and MMT2

delamination of the MMT layers by the surfactant. This increase in surface area was remarkably lost for MMT3 upon thermal treatment due to the combustion of the organic substrate. The addition of NSAg to MMT or MMT-CTAB was accompanied by an apparent decrease in their specific surface area probably due to the occlusion of NSAg in the interparticle pores and the increase in the attraction forces between the clay particles especially in case of organo-functionalized clays. This is in accordance with the results reported for sulphur and amino-functionalized NSAg-MMT which was explained that NSAg are hosted in the pores of MMT [24]. MMT3 shows an increase in its S_{BET} value compared to its parent material MMT2 probably due to the craters formed during the loss of the organic part upon combustion.

SEM micrographs of the NSAg-modified MMT clays (Fig. 7) show the lamellar structure of MMT which is maintained for modified clays. The porosity and crimps of surface structure of the clay samples increased in the order MMT \sim MMT1 $<$ MMT2 $<$ MMT3 $<$ MMT-CTAB which is in accordance with measured S_{BET} . MMT1 shows Ag aggregates in the size range of 500 nm which means that NSAg in MMT1 losses its nano-size. No indication of such behaviour could be observed in organo-functionalized samples which may indicate that NSAg is well occluded within the clay sheets.

Table 2 S_{BET} of MMT and its NSAg-modified samples

Name of sample	Ag%	Expected added surface area of NSAg per gram of clay, m^2		Observed S_{BET} , $\text{m}^2 \text{g}^{-1}$
		5-nm-long cubes	20-nm-long cubes	
MMT	–	–	–	24.5
MMT1	0.042	0.047	0.012	22.4
MMT-CTAB	–	–	–	255
MMT2	0.106	0.118	0.029	70.7
MMT3	0.126	0.14	0.035	153

TEM micrographs of MMT3 (Fig. 8) show the existence of particles of high atomic weight within the size range 8.0–40 nm, probably NSAg, occluded within the MMT sheets. This supports the previous conclusion of caging NSAg within the interparticular confinements of MMT.

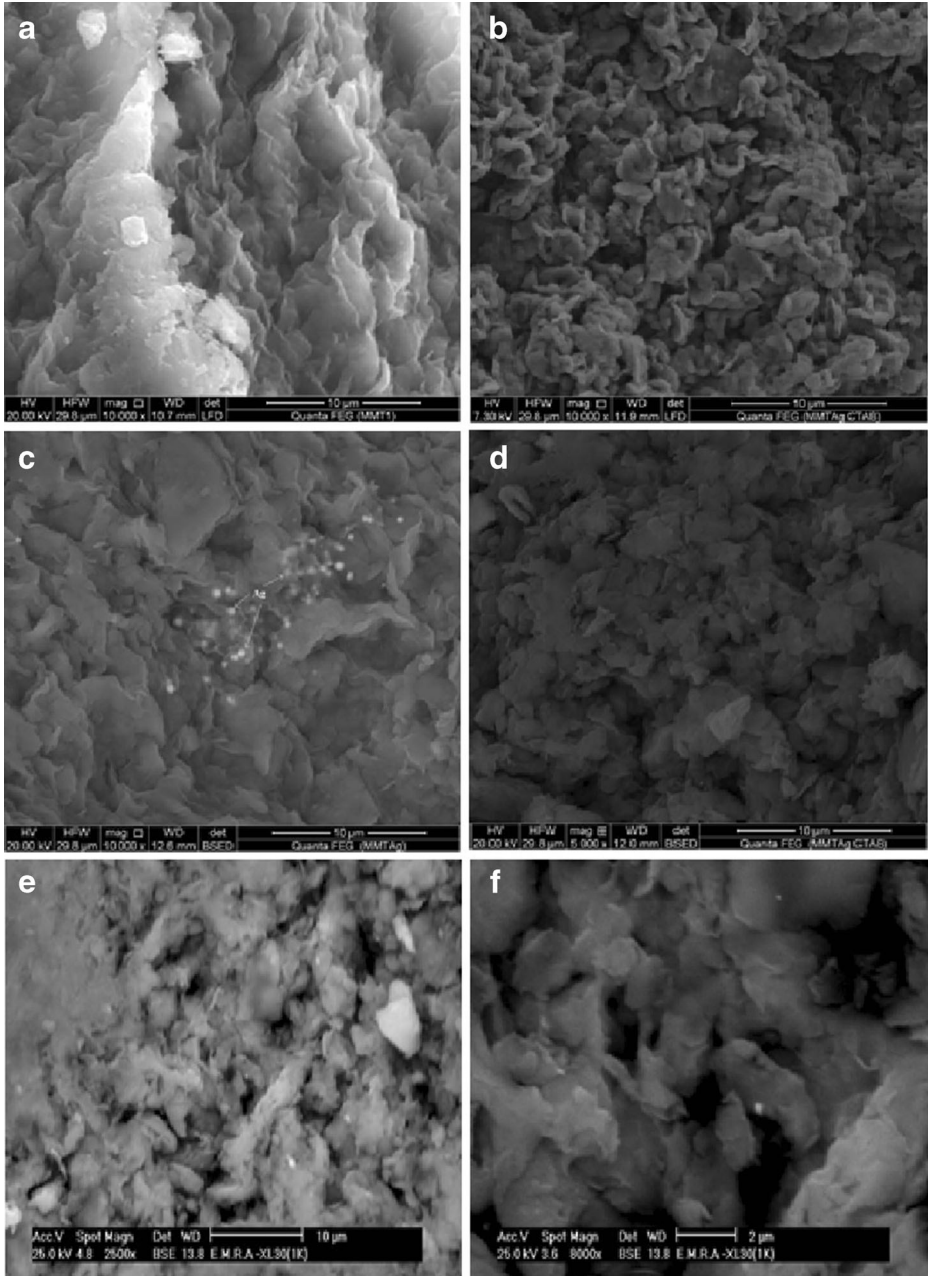


Fig. 7 SEM images of MMT-pure (a), MMT-CTA⁺ (b), MMT1 (c), MMT2 (d) and MMT3 (e, f)

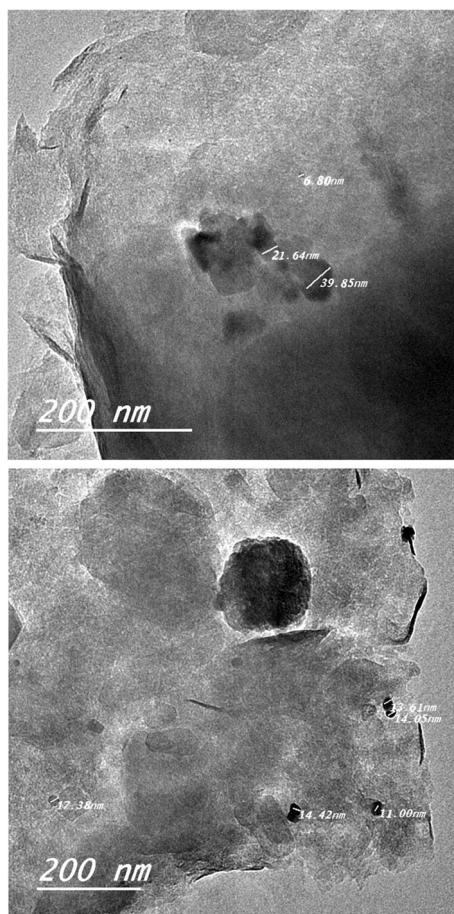


Fig. 8 TEM images of MMT3

Antimicrobial Activity of NSAg-Modified MMT Clays

Antimicrobial Activity Using Cup Plate Method

The antimicrobial activity of NSAg-modified MMT clays, compared with those of MMT and MMT-CTAB, was individually evaluated against *S. aureus*, *E. coli* and *C. albicans* by disc susceptibility test (cup plate method) shown in Table 3. Apparently, the NSAg-modified samples (except for MMT3) exhibited a strong antimicrobial activity whereas the control samples are ineffective. MMT2 shows best antimicrobial activity especially towards *C. albicans* owed to the higher content of NSAg, hybrid properties and the high expansion ability in water compared with MMT1 [43]. The observed antimicrobial activity of MMT2 is observably high when compared with those reported for similar MMT composites [24] and NSAg-gum ghatti [44] which contain up to 7.0 and 3.0–10.0 % NSAg, respectively. The toxic effects of NSAg on microorganisms have been ascribed to Ag^+ ion-related reactive oxygen species production of free radicals that may damage both lipids and DNA [18].

Table 3 Antimicrobial activity of NSAg-modified MMT clays compared with reported results

Sample	Inhibition zone (mm)			Reference
	<i>Staphylococcus aureus</i>	<i>Escherichia coli</i>	<i>Candida albicans</i>	
MMT	–	–	–	Present work, [24]
MMT1	12	14	12	Present work
MMT-CTAB	–	–	–	Present work
MMT2	14	13	16	Present work
MMT3	–	–	–	Present work
S-, NH2- NSAg-MMT	9.8	10.8	–	[24]
NSAg-gum ghatti	12.25	8.0–9.0	–	[44]

Unexpectedly, MMT3, which has the highest concentration of NSAg, appeared ineffective towards the studied microbes which indicate that other factors may influence the antimicrobial activity. The caging of NSAg inside MMT3 particles may limit its release and diffusion through the culture [24]. To prove this concept, about 100 mg of MMT1, MMT2 or MMT3 were shaken in 1 L of distilled water for 24 h, washed by decantation, dried at 110 °C, digested in HF/HNO₃ and analysed for Ag by AAS. The residual concentration of Ag was 0.388, 0.187 and 0.188 %, respectively. This may indicate that the modified clay layers were dispersed in the solution and the denser NSAg aggregates and is concentrated in clay. The order of stability of the NSAg clay composites increase with the order MMT1 < MMT2 < MMT3. Accordingly, the diffusion of MMT3 into solution was observably limited due to the lamellar structure collapse caused by the thermal treatment [41] referring to the reported importance of the release of NSAg from the MMT host for the antimicrobial activity [24, 45].

Antimicrobial Activity Using Plate Count Technique

To explore the antimicrobial activity of MMT3 against *S. aureus*, a CFU was counted instead of the static cup plate method. Compared with *E. coli*, *S. aureus* cells' growth is much more difficult to inhibit, and the bacteria are even harder to be killed, based on the bacterial growth test and viability test results. In Table 4 results obtained from the in vitro tests are reported. As can be seen from data, a significant delay (59 %) in microbial growth was obtained in presence of the MMT3. The pictures in Fig. 9a, b better highlight the different microbial population grew in the various samples. The effects of NSAg immobilized onto MMT were also demonstrated in other recent works of the scientific literature [23, 24, 46]. The hydrophilic cell wall structure of Gram-negative bacteria as

Table 4 Antibacterial activity of MMT3 in comparison to control (*Staphylococcus aureus* culture) using plate count technique

Sample	Absorbance at 660 nm	Number of CFU (10 ⁷ /mL)	Reduction in CFU (%)
Bacterial culture	1.638	2.89	0.0
MMT3	1.436	1.18	59.17

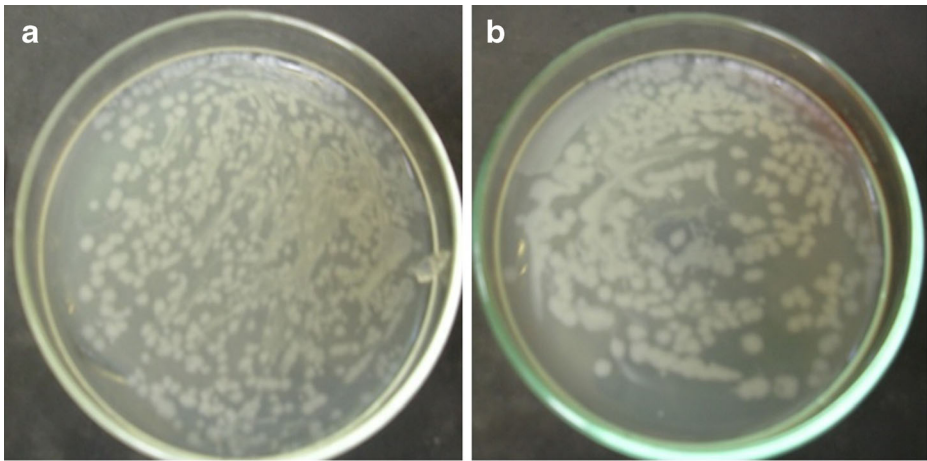


Fig. 9 *Staphylococcus aureus* colony forming units of untreated control (a) and MMT3 (b)

Pseudomonas spp. is essentially constituted of lipopolysaccharides that attract toward the weak positive charge available on silver ions, thus allowing the silver-based antimicrobial nano-particles to be effective [47]. The characteristic hydrophilic surface of the MMT host may play an important role in approaching together the microorganism and the NSAg in the aqueous media. This may be supported by the previous experimental evidence that demonstrated that silver ion release is governed by water transport properties of the film, by nature and quantity of the silver particles and their distribution within the matrix [11, 12]. Further work is still necessary to better correlate silver diffusion mechanism to its antimicrobial activity.

Conclusion

This study reports a facile and biosynthesis of silver nano-particles with a size range ~5.4–21.5 nm from silver nitrate using the bacteria *M. bovicus* isolated from local soil. The produced NSAg was proved to be immobilized onto MMT, CTAB-MMT, to capture NSAg within the interparticular confinements of the clay.

Presence of CTAB in the MMT structure increased the occlusion of NSAg and kept its size and structure without noticeable change. Thermal treatment of the MMT increased its composition stability while it diminished the NSAg release and MMT layer dispersion as well. The efficiency of antimicrobial activity towards the Gram-negative and Gram-positive bacteria and fungus was evidenced by NSAg-MMT and in particular NSAg-CTAB-MMT via the dispersion of NSAg. MMT3 could inhibit the bacterial growth by using the CFU method. As the particle size of the nano-particles can be reserved, this method can be implemented for the large-scale production of antimicrobial composites due to the availability of low-cost clay host. The hydroxyl groups of the clay surface were suggested to facilitate the approach of both NSAg and the microorganisms together enabling their interaction. The adopted method is compatible with green chemistry principles as the *M. bovicus* and MMT serve as a reductant and stabilizer, respectively, for the synthesis of nano-composite having strong antimicrobial activity.

References

1. UN (2013b). Statistical annex: millennium development goals, targets and indicators. <http://unstats.un.org/unsd/mdg/Default.aspx>. Accessed 24 Mar 2014.
2. Guidelines for Drinking-water Quality (2008). *Incorporating the first and second addenda, recommendations (pp 121, 1)* (Third ed.,). Geneva:WHO.
3. Obasohan, E. E., Agbonlahor, D. E., & Obano, E. E. (2010). Water pollution: a review of microbial quality and health concerns of water, sediment and fish in the aquatic ecosystem. *African Journal of Biotechnology*, *9*(4), 423–427.
4. Osman, G. A., Hassan, H. M., & Kamel, M. M. (2011). Resistance and sensitivity of some bacterial strains isolated from hospital wastewater and Nile water using chlorination and some antibiotics in Cairo (Egypt). *Journal of American Science*, *7*(9), 1033–1041.
5. Khandelwal, N., Kaur, G., Kumara, N., & Tiwari, A. (2014). Application of silver nanoparticles in viral inhibition: a new hope for antivirals. *Digest Journal of Nanomaterials and Biostructures*, *9*, 175–186.
6. Rispaill, N., De Matteis, L., Santos, R., Miguel, A. S., Custardoy, L., Testillano, P. S., Risueño, M. C., Pérez-de-Luque, A., Maycock, C., Fevereiro, P., Oliva, A., Fernández-Pacheco, R., Ibarra, M. R., de la Fuente, J. M., Marquina, C., Rubiales, D., & Prats, E. (2014). Quantum dot and superparamagnetic nanoparticle interaction with pathogenic fungi: internalization and toxicity profile. *ACS Applied Materials & Interfaces*, *6*(12), 9100–9110.
7. Swain, P., Nayak, S. K., Sasmal, A., Behera, T., Barik, S. K., Swain, S. K., Mishra, S. S., Sen, A. K., Das, J. K., & Jayasankar, P. (2014). Antimicrobial activity of metal based nanoparticles against microbes associated with diseases in aquaculture. *World Journal of Microbiology and Biotechnology*, *30*, 2491–2502.
8. Rizzello, L., Cingolani, R., & Pompa, P. P. (2013). Nanotechnology tools for antibacterial materials. *Nanomedicine*, *8*(5), 807–821.
9. Velázquez-Velázquez, J. L., Santos-Flores, A., Araujo-Meléndez, J., Sánchez-Sánchez, R., Velasquillo, C., González, C., Martínez-Castañón, G., & Martínez-Gutierrez, F. (2015). Anti-biofilm and cytotoxicity activity of impregnated dressings with silver nanoparticles. *Materials Science and Engineering: C*, *49*, 604–611.
10. Wijnhoven, S. W. P., Peijnenburg, W. J. G. M., Herberts, C. A., Hagens, W. I., Oomen, A. G., Heugens, E. H. W., Roszek, B., Bisschops, J., Gosens, I., Van De Meent, D., Dekkers, S., De Jong, W. H., Van Zijverden, M., Sips, A. J., & Geertsma, R. E. (2009). Nano-silver—a review of available data and knowledge gaps in human and environmental risk assessment. *Anotoxicology*, *3*(2), 109–138.
11. Freire, P. L. L., Stamford, T. C. M., Albuquerque, A. J. R., Sampaio, F. C., Cavalcante, H. M. M., Macedo, R. O., Galembeck, A., Flores, M. A. P., & Rosenblatt, A. (2015). Action of silver nanoparticles towards biological systems: cytotoxicity evaluation using hen's egg test and inhibition of *Streptococcus mutans* biofilm formation. *International Journal of Antimicrobial Agents*, *45*, 183–187.
12. Tolaymat, T., El Badawy, A., Genaidy, A., Scheckel, K., Luxton, T., & Suidan, M. (2010). An evidence-based environmental perspective of manufactured silver nanoparticle in syntheses and applications: a systematic review and critical appraisal of peer-reviewed scientific papers. *The Science of the Total Environment*, *408*(5), 999–1006.
13. Vigneshwaran, N., Kathe, A. A., Varadarajan, P. V., Nachane, R. P., & Alasubramanya, A. (2007). Silver-protein (core-shell) nanoparticle production using spent mushroom substrate. *Langmuir*, *23*, 7113–7117.
14. Kalimuthu, K., Babu, R. S., Venkataraman, D., Bilal, M., & Gurunathan, S. (2008). Biosynthesis of silver nanocrystals by *Bacillus licheniformis*. *Colloids and Surfaces B: Biointerfaces*, *65*, 150–153.
15. Bhainsa, K. C., & D'Souza, S. F. (2006). Extracellular biosynthesis of silver nanoparticles using the fungus *Aspergillus fumigatus*. *Colloids and Surfaces B: Biointerfaces*, *47*, 160–164.
16. Mukherjee, P., Roy, M., Mandal, B. P., Dey, G. K., Mukherjee, P. K., Ghatak, J., Tyagi, A. K., & Kale, S. P. (2008). Green synthesis of highly stabilized nanocrystalline silver particles by a nonpathogenic and agriculturally important fungus *T. asperellum*. *Nanotechnology*, *19*, 075103.
17. Khan, M., Khan, M., Adil, S. F., Tahir, M. N., Tremel, W., Alkhatlan, H. Z., Al-Warthan, A., & Siddiqui, M. R. (2013). Green synthesis of silver nanoparticles mediated by *Pulicaria glutinosa* extract. *International Journal of Nanomedicine*, *8*, 1507–1516.
18. Kovvuru, P., Mancilla, P. E., Shirole, A. B., Murray, T. M., Begley, T. J., & Reliene, R. (2014). Oral ingestion of silver nanoparticles induces genomic instability and DNA damage in multiple tissues, oral ingestion of silver nanoparticles induces genomic instability and DNA damage in multiple tissues. *Nanotoxicology*. doi:10.3109/17435390.2014.902520.
19. Jiang, J., Oberdörster, G., & Biswas, P. (2009). Characterization of size, surface charge, and agglomeration state of nanoparticle dispersions for toxicological studies. *Journal of Nanoparticle Research*, *11*, 77–89.
20. El Badawy, A., Luxton, T., Silva, R., Scheckel, K., Suidan, M., & Tolaymat, T. (2010). Impact of environmental conditions (pH, ionic strength, and electrolyte type) on the surface charge and aggregation of NSAg suspensions. *Environmental Science & Technology*, *44*(4), 1260–1266.

21. Benn, T. M., & Westerhoff, P. (2008). Nanoparticle silver released into water from commercially available sock fabrics. *Environmental Science & Technology*, *42*, 4133–4139.
22. Shameli, K., Ahmad, M. B., Yunus, W. M. W., Ibrahim, N. A., Gharayebi, Y., & Sedaghat, S. (2010). Synthesis of silver/montmorillonite nanocomposites using γ -irradiation. *International Journal of Nanomedicine*, *5*, 1067–1077.
23. Lavorgna, M., Attianese, I., Buonocore, G. G., Conte, A., Del Nobile, M. A., Tescione, F., & Amendola, E. (2014). MMT-supported Ag nanoparticles for chitosan nanocomposites: structural properties and antibacterial activity. *Carbohydrate Polymers*, *102*, 385–392.
24. Tian, L., Oulian, L., Zhiyuan, L., Liuimei, H., & Xiaosheng, W. (2014). Preparation and characterization of silver loaded montmorillonite modified with sulfur amino acid. *Applied Surface Science*, *305*, 386–395.
25. Gillott, J. E. (1968). *Clay in engineering geology. (Chapter 5)* (1st ed.,). Amsterdam:Elsevier.
26. Vazquez, A., López, M., Kortaberria, G., Martín, L., & Mondragon, I. (2008). Modification of montmorillonite with cationic surfactants. Thermal and chemical analysis including CEC determination. *Applied Clay Science*, *41*, 24–36.
27. Srinivasan, D., Nathan, S., Suresh, T., & Lakshmana, P. P. (2001). Antimicrobial activity of certain Indian medicinal plants used in folkloric medicine. *Journal of Ethnopharmacology*, *74*, 217–220.
28. Gupta, D., Khare, S. K., & Laha, A. (2004). Antimicrobial properties of natural dyes against Gram-negative bacteria. *Coloration Technology*, *120*, 167–171.
29. Duhan, S., Devi, S., & Kumar, S. (2010). Synthesis of composite based on nano sized silver particles hosted on silica networks. *International Journal of Electrical Engineering*, *2*(1), 225–228.
30. Mie, G. (1908). Beiträge zur Optik trüber Medien, speziell kolloidaler Metallosungen. *Annalen der Physik*, *25*, 377.
31. Wang, H., Law, N., Pearson, G., van Dongen, B. E., Jarvis, R. M., Goodacre, R., & Lloyd, J. R. (2010). Impact of silver (I) on the metabolism of *Shewanella oneidensis*. *Journal of Bacteriology*, *192*(4), 1143–1150.
32. Zhu, J., Zhu, L., Zhu, R., & Chen, B. (2008). Microstructure of organobentonites in water and the effect of steric hindrance on the uptake of organic compounds. *Clays and Clay Minerals*, *56*(2), 144–154.
33. (1995) Composition and mineralogy of clay minerals. In: B. Velde (Ed.), *Origin and mineralogy of clays* (pp. 27–33). Berlin: Springer-Verlag.
34. Lagaly, G., Ogawa, M., & Dekany, I. (2006). Clay mineral organic interactions. In F. Bergaya, B. K. G. Theng, & G. Lagaly (Eds.), *Handbook of clay science* (pp. 309–377). Amsterdam: Elsevier.
35. He, H., Frost, R. L., Bostrom, T., Yuan, P., Duong, L., Yang, D., Xi, Y., & Klopogge, J. T. (2006). Changes in the morphology of organoclays with HDTMA+ surfactant loading. *Applied Clay Science*, *31*, 262–271.
36. Grim, R. E. (1968). *Clay mineralogy* (p. 288). New York, USA:Mc Graw Hill Company.
37. Ferraro, J. R. (1982). *The Sadtler infrared spectra handbook of minerals and clays* (pp. 354–356). Philadelphia, Pennsylvania:Sadtler Research Laboratories.
38. Letaief, S., Casal, B., Aranda, P., Martín-Luengo, M. A., & Ruiz-Hitzky, E. (2003). Fe-containing pillared clays as catalysts for phenol hydroxylation. *Applied Clay Science*, *22*, 263–277.
39. Lambert, J. B., Shurvell, H. F., Lighter, D. A., & Cooks, R. G. (1998). *Organic structural spectroscopy*. New Jersey:Prentice-Hall.
40. Fatimah, I., & Huda, T. (2013). Preparation of cetyltrimethylammonium intercalated Indonesian montmorillonite for adsorption of toluene. *Applied Clay Science*, *74*, 115–120.
41. Harris, D. J., Bonagamba, T. J., & Schmidt-Rohr, K. (1999). Conformation of poly(ethylene oxide) intercalated in clay and MoS₂ studied by two-dimensional double-quantum NMR. *Macromolecules*, *32*, 6718–6724.
42. Xie, W., Gao, Z., Pan, W., Huner, D., Singh, A., & Vaia, R. (2001). Thermal degradation chemistry of alkyl quaternary ammonium montmorillonite. *Chemistry of Materials*, *13*(9), 2979–2990.
43. Zhu, Z. J., Wang, T., Zhu, R., Ge, F., Yuan, P., & He, H. (2011). Expansion characteristics of organo montmorillonites during the intercalation, aging, drying and rehydration processes: effect of surfactant/CEC ratio. *Colloids and Surfaces A: Physicochemical and Engineering Aspects*, *384*(1–3), 401–407.
44. Kora, A. J., Beedu, S. R., & Jayaraman, A. (2012). Size-controlled green synthesis of silver nanoparticles mediated by gum ghatti (*Anogeissus latifolia*) and its biological activity. *Organic and Medicinal Chemistry Letters*, *2*, 17.
45. Lin, J. J., Lin, W. C., Li, S. D., Lin, C. Y., & Hsu, S. H. (2013). Evaluation of the antibacterial activity and biocompatibility for Ag NPs immobilized on nano silicate platelets. *ACS appl Mathematical Intelligence*, *5*, 433–443.
46. Inconorato, A. L., Conte, A., Buonocore, G. G., & Del Nobile, M. A. (2011). Agar hydrogel with silver nanoparticles to prolong the shelf life of Fior di Latte cheese. *Journal of Dairy Science*, *94*, 1697–1704.
47. Bezic, N., Skocibusic, M., Dinkic, V., & Radonic, A. (2003). Composition and antimicrobial activity of *Achillea clavennae* L. essential oil. *Phytotherapy Research*, *17*, 1037–1040.